



HAL
open science

A Predicted Dearth of Majority Hypervolatile Ices in Oort Cloud Comets

C. M. Lisse, G. R. Gladstone, L. A. Young, D. P. Cruikshank, S. A. Sandford, B. Schmitt, S. A. Stern, H. A. Weaver, O. Umurhan, Y. J. Pendleton, et al.

► **To cite this version:**

C. M. Lisse, G. R. Gladstone, L. A. Young, D. P. Cruikshank, S. A. Sandford, et al.. A Predicted Dearth of Majority Hypervolatile Ices in Oort Cloud Comets. *The Planetary Science Journal*, 2022, 3, 10.3847/PSJ/ac6097 . insu-03690855

HAL Id: insu-03690855

<https://insu.hal.science/insu-03690855>

Submitted on 8 Jun 2022

HAL is a multi-disciplinary open access archive for the deposit and dissemination of scientific research documents, whether they are published or not. The documents may come from teaching and research institutions in France or abroad, or from public or private research centers.

L'archive ouverte pluridisciplinaire **HAL**, est destinée au dépôt et à la diffusion de documents scientifiques de niveau recherche, publiés ou non, émanant des établissements d'enseignement et de recherche français ou étrangers, des laboratoires publics ou privés.



Distributed under a Creative Commons Attribution 4.0 International License



A Predicted Dearth of Majority Hypervolatile Ices in Oort Cloud Comets

C. M. Lisse¹ , G. R. Gladstone^{2,3} , L. A. Young⁴ , D. P. Cruikshank⁵ , S. A. Sandford⁶ , B. Schmitt⁷ , S. A. Stern⁴ , H. A. Weaver¹ , O. Umurhan⁶ , Y. J. Pendleton⁸ , J. T. Keane⁹ , J. M. Parker⁴ , R. P. Binzel¹⁰ , A. M. Earle¹⁰ , M. Horanyi¹¹ , M. El-Maarry¹² , A. F. Cheng¹ , J. M. Moore⁶ , W. B. McKinnon¹³ , W. M. Grundy¹⁴ , J. J. Kavelaars¹⁵ , I. R. Linscott¹⁶ , W. Lyra¹⁷ , B. L. Lewis^{18,19} , D. T. Britt⁵ , J. R. Spencer⁴ , C. B. Olkin⁴ , R. L. McNutt¹ , H. A. Elliott^{2,3} , N. Dello-Russo¹ , J. K. Steckloff^{20,21} , M. Neveu^{22,23} , and O. Mousis²⁴

¹ Space Exploration Sector, Johns Hopkins University Applied Physics Laboratory, 11100 Johns Hopkins Road, Laurel, MD 20723, USA; carey.lisse@jhuapl.edu, hal.weaver@jhuapl.edu, ralph.mcnuitt@jhuapl.edu, andy.cheng@jhuapl.edu, neil.dello.russo@jhuapl.edu

² Southwest Research Institute, San Antonio, TX 28510, USA; randy.gladstone@swri.org, helliott@swri.edu

³ Physics and Astronomy Department, University of Texas at San Antonio, San Antonio, TX 78249, USA

⁴ Southwest Research Institute, Boulder, CO 80302, USA; alan@boulder.swri.edu, layoung@boulder.swri.edu, joel@boulder.swri.edu, colkin@boulder.swri.edu, spencer@boulder.swri.edu

⁵ Department of Physics, University of Central Florida, Orlando, FL 32816, USA; dpcruikshank@comcast.net, dbritt@ucf.edu

⁶ Astrophysics Branch, Space Sciences and Astrobiology Division, NASA/Ames Research Center, Moffett Field, CA 94035, USA; scott.a.sandford@nasa.gov, orkan.m.umurhan@nasa.gov

⁷ Université Grenoble Alpes, CNRS, CNES, Institut de Planétologie et Astrophysique de Grenoble, Grenoble, France bernard.schmitt@univ-grenoble-alpes.fr

⁸ Space Science and Astrobiology Division, NASA/Ames Research Center, Moffett Field, CA 94035, USA; pendletonyvonne@gmail.com, jeff.moore.mail@gmail.com

⁹ Astrophysics and Space Sciences Section, Jet Propulsion Laboratory/Caltech, Pasadena, CA 91109, USA; jkeane@caltech.edu

¹⁰ Department of Earth, Atmospheric, and Planetary Sciences, Massachusetts Institute of Technology, Cambridge, MA 02139, USA; rpb@mit.edu, aearle@mit.edu

¹¹ Laboratory for Atmospheric & Space Physics, University of Colorado, Boulder, CO 80303, USA; mihaly.horanyi@lasp.colorado.edu

¹² Birkbeck, University of London, WC1E 7HX, London, UK; m.elmaarry@bbk.ac.uk

¹³ Department of Earth and Planetary Sciences and McDonnell Center for Space Sciences, One Brookings Drive, Washington University, St. Louis, MO 63130, USA; mckinnon@wustl.edu

¹⁴ Lowell Observatory, 1400 West Mars Hill Road, Flagstaff, AZ 86001, USA; W.Grundy@lowell.edu

¹⁵ NRC Herzberg Inst of Astrophysics, 5071 W Saanich Road, Victoria BC V9E 2E7 BC, Canada; JJ.Kavelaars@nrc-cnrc.gc.ca

¹⁶ Hansen Experimental Physics Laboratory, Stanford University, Stanford, CA 94305-9515, USA; linscott@stanford.edu

¹⁷ Department of Astronomy, New Mexico State University, PO BOX 30001, MSC 4500, Las Cruces, NM 88003-8001, USA; wlyra@nmsu.edu

¹⁸ Department of Astronomy, Columbia University, 550 W. 120th Street, New York, NY 10027, USA; bl2124@columbia.edu

¹⁹ Division of Astronomy and Astrophysics, University of California, Los Angeles, 475 Portola Plaza, Los Angeles, CA 90025, USA

²⁰ Planetary Science Institute, Tucson, AZ 85719, USA; jordan@psi.edu

²¹ Department of Aerospace Engineering and Engineering Mechanics, University of Texas at Austin, Austin, TX 78712, USA

²² Department of Astronomy, University of Maryland College Park, College Park, MD 20742, USA; marc.f.neveu@nasa.gov

²³ NASA/Goddard Space Flight Center, Planetary Environments Laboratory, Greenbelt, MD 20771, USA

²⁴ Aix-Marseille Université, CNRS, CNES, LAM, Marseille, France; olivier.mousis@lam.fr

Received 2021 September 1; revised 2022 February 16; accepted 2022 March 14; published 2022 May 17

Abstract

We present new, ice species-specific New Horizons/Alice upper gas coma production limits from the 2019 January 1 MU69/Arrokoth flyby of Gladstone et al. and use them to make predictions about the rarity of majority hypervolatile (CO, N₂, CH₄) ices in Kuiper Belt objects and Oort Cloud comets. These predictions have a number of important implications for the study of the Oort Cloud, including the determination of hypervolatile-rich comets as the first objects emplaced into the Oort Cloud, the measurement of CO/N₂/CH₄ abundance ratios in the protoplanetary disk from hypervolatile-rich comets, and population statistical constraints on early (<20 Myr) planetary aggregation driven versus later (>50 Myr) planetary migration driven emplacement of objects into the Oort Cloud. They imply that the phenomenon of ultradistant active comets like C/2017K2 should be rare, and thus not a general characteristic of all comets. They also suggest that interstellar object 2I/Borisov may not have originated in a planetary system that was inordinately CO rich, but rather could have been ejected onto an interstellar trajectory very early in its natal system's history.

Unified Astronomy Thesaurus concepts: [Pluto \(1267\)](#); [Trans-Neptunian objects \(1705\)](#); [Oort cloud objects \(1158\)](#); [Long period comets \(933\)](#); [Comets \(280\)](#); [Ice destruction \(2091\)](#); [Ice formation \(2092\)](#); [Comae \(271\)](#); [Neutral coma gases \(2158\)](#)

1. Introduction

Lisse et al. (2021, hereafter Lisse+21) presented state-of-the-art saturation vapor pressure (P_{sat}) and gas production rate (Q_{gas}) curves for ices expected in Kuiper Belt objects (KBOs) like 2014 MU₆₉ (hereafter Arrokoth) and Pluto. These curves

were informed by the ices found in comets and on the surfaces of outer solar system Centaur, Trojan, and KBO bodies. The primary purpose for calculating these P_{sat} and Q_{gas} curves was to determine which chemical species could be present in abundance in Arrokoth given the 3σ nondetection upper limit of H coma gas production of 10^{24} mol s⁻¹ from New Horizons (NH) Alice instrument airglow observations of Arrokoth (Stern et al. 2019). Assuming that the H production upper limit was a good proxy for the production rate limits of ices found in other small solar system icy bodies, Lisse+21 went on to show that

there could not be any hypervolatile (e.g., N_2 , CO , CH_4) or mesovolatile (C_2H_6 , C_3H_8 , C_6H_6 , SO_2 , H_2S , etc.) pure ice species in any substantial abundance on the surface of Arrokoth. Rather, refractory hydrogen-bonded ice species such as water, methanol, HCN, and ammonia that remain thermally stable against sublimation into space over Gyr at the local surface temperatures should be in residence.²⁵ This finding was consistent with the NH/LEISA and NH/MVIC findings of a surface uniformly rich in tholins, methanol ice, and likely water ice (Grundy et al. 2020).

Steckloff et al. (2021, hereafter Steckloff+21) used P_{sat} and Q_{gas} curves, coupled with a simple one-dimensional model of comet interior processes (Steckloff et al. 2015, 2016), to model Arrokoth’s hypervolatile ice content. They found that insolation would deplete Arrokoth of pure hypervolatile ices within the first 10–100 Myr (with little variance due to the amount of short-lived radioactive nuclides), consistent with the lack of hypervolatile activity reported by Lisse+21. Steckloff+21’s results were subsequently confirmed by the ~ 10 Myr loss time for CO from a 30 km diameter body by Davidsson (2021, hereafter Davidsson+21) and the 24 ± 3 Myr hypervolatile loss time from Arrokoth found by Prialnik (2021, hereafter Prialnik+21).

In a companion paper, Gladstone et al. (2022) present new analyses of an NH/Alice apulse observation of the Sun to determine upper limits to gas production rates for the ice species studied in Lisse+21—and these are all at the $\sim 0.1\text{--}1 \times 10^{29}$ molecule s^{-1} level, higher than the H-atom proxy number quoted in Lisse+21. These new species-specific values, while high compared to the $Q_{gas,H}$, nevertheless support the arguments made and conclusions drawn in Lisse+21 and Steckloff+21 concerning the lack of pure hypervolatile outgassing activity, and thus the lack of pure hypervolatile species present, on Arrokoth in the present-day thermal environment. Here we correct and update the literature argument for the nonpresence of pure hypervolatile species by presenting the updated individual species limits (Figure 1).

2. A Predicted Dearth of Near-pure Hypervolatile Ices in the Oort Cloud

2.1. The Origin and Sources of Hypervolatile Ices

By considering the provenance and very early history of these hypervolatile and refractory ices, we can draw another important solar system ices prediction from these analyses. The hypervolatile ices can be identified as Ehrenfreund et al.’s (2001) small, low-polarity ices, like CO , N_2 , O_2 , and CH_4 . Unable to bind well to dust grain surfaces, such “apolar” ice molecules form mainly from gas-phase reactions and condense directly to ice in cold molecular clouds at extremely cold temperatures ($\sim 10\text{--}20$ K), where thermal energy can be dominated by van der Waals interactions. By contrast, Ehrenfreund et al.’s (2001) more massive and strongly polar ices, termed here as “refractory” ices, adhere readily to grain surfaces at temperatures upwards of 100 K and are thus efficiently formed as products of heterogeneous grain catalysis on the surfaces of dust grains in clouds.

Often forgotten in solar system studies is that the initial feedstock of gas and dust in the cold molecular cloud (that

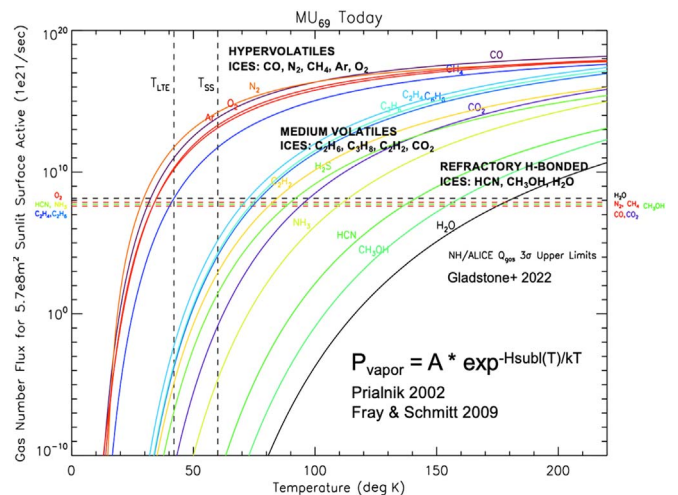


Figure 1. Species-specific $3\sigma Q_{gas}$ production upper limits for Arrokoth, as determined by Gladstone et al. (2022; horizontal colored dashed lines at $10^7\text{--}10^8 \times 10^{21}$ molecules s^{-1}). Also plotted on the same scale are the gas production rates for different expected icy species found in comets and KBOs (colored curves), as well as the local LTE temperature at 45 au from the Sun for Arrokoth and its subsolar (noon-time) temperature (vertical dashed lines). Hypervolatile species like N_2 , CO , and CH_4 (red) violate the new NH/Alice upper detection limits by 6–8 orders of magnitude. After Lisse+21.

became the protosolar nebula), like the bulk interstellar medium (ISM), had a dust-to-gas-mass ratio $D/G \sim 0.01$, 2 orders of magnitude smaller than the $D/G \sim 3^{+4/-2}$ regime of solid bodies in the solar system today (Ishii et al. 2018; Zhukovska et al. 2018; Choukroun et al. 2020). Similarly, in the very early, gas-dominated solar system, with a solar C/O ratio = 0.54, one would expect ~ 1 H_2O molecule for 1 CO molecule, rather than the 5–1000 H_2O molecules for 1 CO we see today in comets (i.e., $Q_{CO}/Q_{H_2O} = 0.1\%$ to 20%, not $\sim 100\%$; Bockelée-Morvan et al. 2004; Bockelée-Morvan & Biver 2016; Mumma & Charnley 2011). The key point here is that easily vaporized hypervolatile apolar ice loss in the very early solar system (upwards of 99% of the original gas content) was a normal and expected occurrence concomitant with loss of gas from the circumstellar protoplanetary disk to the ISM at 5–10 Myr (Williams & Cieza 2011; Ercolano & Pascucci 2017), and necessary to produce the small icy outer solar system bodies we know today.

However, the only direct evidence we see for abundant hypervolatile ices in today’s solar system is in the atmospheres of the giant planets and their largest moons and on the surfaces of the largest KBOs (Barucci et al. 2008, 2011; Brown 2012). These are all bodies capable of supporting gravitationally bound atmospheres (Schaller & Brown 2007; Zahnle & Catling 2017; Young et al. 2020). Like Arrokoth, small KBOs and Centaurs show evidence for methanol and water ice, (Cruikshank et al. 1998; Barucci et al. 2008, 2011) but not hypervolatiles. Comets, which are descended from in-scattered modern KBOs (the short-period comets; Lisse 2002; Jewitt 2009; Dones et al. 2015) or ancient outwardly scattered KBOs (Oort Cloud comets; Brassier & Morbidelli 2013; Garrod 2019; Morbidelli & Nesvorniy 2020) do not show any obvious surface absorption features due to ices, except for the rare small patch of water ice or frost (Sunshine et al. 2006; Fornasier et al. 2015, 2019; Quirico et al. 2015, 2016; Lisse et al. 2017).

²⁵ To be precise, the curves track the behavior of pure ices and almost pure ($>90\%$ one species) ices. More mixed phases usually have much more complicated behaviors and, when such phases are determined to be present, will require individual study as treatment.

Cometary comae do show evidence for low, but finite levels of hypervolatile species (CO at 0.5%–25% versus water, N₂ at 0.1%–0.3% versus water, CH₄ at 0.2%–1.0% versus water, and [CO + CO₂] at ~20% versus water; Bockelée-Morvan et al. 2004; Mumma & Charnley 2011; A’Hearn et al. 2012; Bockelée-Morvan & Biver 2016). This implies that there must be some reservoir for them in these objects—but it cannot be in deeply held near-pure hypervolatile ice phases. Not only is this highly unlikely given the study of cometary thermal timescales for ~1–10 km sized cometary nuclei with lag deposits published by Davidsson+21 and Steckloff+21, bolstered by the modeling of Arrokoth’s ice loss performed by Prialnik+21—it would also take deeply buried regions held at ~15 K since the beginning of the solar system 4.56 Gyr ago, coupled with an enormous, aphysical lag delay, to force this to happen, contrary to the modern 30–40 K core temperatures of Arrokoth determined by Davidsson+21, Lisse+21, Prialnik+21, Steckloff+21, and Umruhan et al. (2022).²⁶ The existence of deeply buried pure hypervolatile ices is also contrary to the lack of substantial hypervolatile emission, such as CO, from end member objects 45P/Honda–Mrkos–Pajdušáková, 46P/Wirtanen, and 103P/Hartley 2 (small comets near the end of their lives emitting chunks of their cores; A’Hearn et al. 2011; DiSanti et al. 2017; Steckloff & Samarasinha 2018). For example, a massive landslide is thought to have exposed the interior of Comet 103P/Hartley 2 only ~3 decades ago (Steckloff et al. 2016); however, the EPOXI mission detected no evidence of strong hypervolatile emission (A’Hearn et al. 2011).

Neither was any marked increase in hypervolatile emission seen from the recently split comets 73P/SW3 (Dello Russo et al. 2007) nor from 17P/Holmes (Dello Russo et al. 2008), again showing from direct observational studies that the cores/interiors of Jupiter-family comets do not contain any large amount of pure hypervolatile ices “hidden down deep.”²⁷ Instead the low but finite level of hypervolatile ices seen in cometary comae is thought to be due to their inclusion as minority impurities in bulk majority water ice and CO₂ ice phases (Jewitt 2009; Lisse+21; Davidsson+21), and it is from these phases that it can be released via thermal, sputtering, or collisional processes (Kral et al. 2021 and references therein).

²⁶ Another thermal loss timescale on the order of 4 Gyr has also recently been published by Kral et al. (2021), but this model utilized an aphysical thermal diffusivity = $10^{-10} \text{ m}^2 \text{ s}^{-2}$, which is more than 2 orders of magnitude lower than that of the most insulating solid material currently known, aerogel, and more than 3 orders of magnitude lower than the parameter values used by Davidsson+21, Prialnik+21, and Steckloff+21 in their models. Scaling the 4 Gyr timescale by a factor of 1/300 to correct for the thermal diffusivity error, the Kral et al. timescales become consistent with the 10–20 Myr timescales for loss of all pure CO/N₂/CH₄-like ices.

²⁷ Instead, we follow the arguments of Iro et al. (2003) and Jewitt (2009) that the hypervolatiles and moderately volatile species in Centaurs and short-period comets are protectively stored in H₂O ice matrices—first at high concentrations in cold ($T < 80 \text{ K}$) amorphous water ice composites, then in lower concentrations in warmer $T > 100 \text{ K}$ crystalline water ice matrices limited by the maximum interlattice “pore space” trapping capability of the crystallite. Li et al. (2020), using the Hubble Space Telescope (HST), verified the lack of activity of Centaurs beyond 10 au. This is consistent with the early work of Prialnik et al. (1987) who argued that the presence of amorphous ice within the subsurface of comets—inferred from observations of outgassing at surprisingly large heliocentric distances (5.8–11.4 au) and attributed to the annealing of amorphous ice as comets first enter the inner solar system (Prialnik & Bar-Nun 1990, 1992; Meech et al. 2009)—provides a clear constraint on the maximum parent body temperatures ($T < 135 \text{ K}$) experienced over long ($\gg 100 \text{ Myr}$) comet lifetimes. The total $Q(\text{CO} + \text{CO}_2)$ of comets is also suspiciously close to the ~20% carrying capacity of crystalline water ice (A’Hearn et al. 2011).

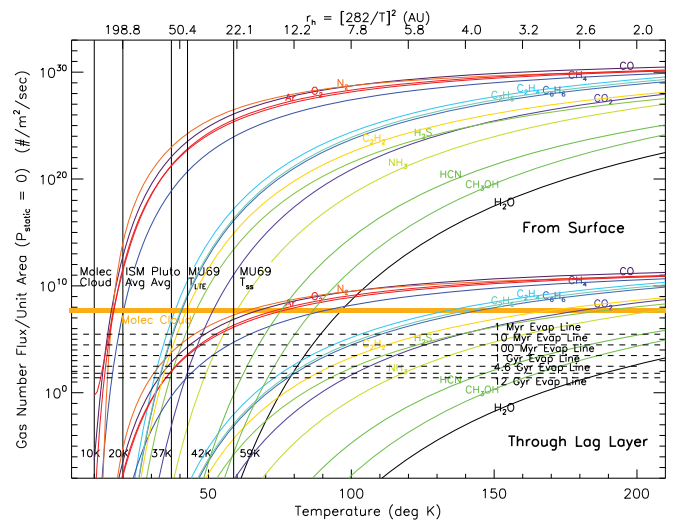


Figure 2. Species-specific Q_{gas} vs. temperature curves for species expected in comets and KBOs (upper colored curves). Horizontal dashed lines: values of the thermally driven outgassing rates at which an icy species is depleted in 1, 10, 100, 1000, 4600, and 12,000 Myr for an Arrokoth-sized body. Upper colored curves: loss rates of a piece of surface ice evaporating into free space. Lower colored curves: the much slower loss rates for the same species, after allowing for an overlying lag layer with thermal diffusivity = $3 \times 10^{-7} \text{ m}^2 \text{ s}^{-1}$ impeding the flow of heat and gas into free space from the interior (Davidsson+21, Steckloff+21, Prialnik+21). Top axis: heliocentric distance from the Sun for a blackbody at local thermal equilibrium temperature T . From these curves and constraints, one can see that hypervolatile ices CO, N₂, and CH₄ are stable in cold, dense molecular clouds and in modern KBOs residing beyond ~100 au from the Sun, but were lost by ~20 Myr after Arrokoth’s formation. One can also see that mesostable ices like CO₂, while easily removed from the surface, can remain stably at depth inside a KBO for more than the age of the solar system.

2.2. Small Outer Solar System Body Hypervolatile Ice Evolution

The lack of abundant near-pure hypervolatile ices in outer solar system bodies, except the very largest with gravitationally bound atmospheres, can be explained by thermal processing effects. After the initial condensation of ices and small icy bodies in the early molecular cloud/T Tauri star/protoplanetary disk phases, another important epoch of the early solar system was the so-called “disk clearing” time, when enough of the gas (~90% or more) was removed from the solar system’s T Tauri accretion disk for it to become optically thin to optical radiation out as far as the Kuiper Belt. In Lisse+21 this was termed “morning coming to the Kuiper Belt,” and by Steckloff+21 as the dawn of the “Sublimative Period” of the Kuiper Belt. Lasting for the first 10–50 Myr of the solar system (~20 Myr for Arrokoth but depending on object size; Steckloff+21; Prialnik+21), the Sublimative Period led to a sudden spike in the local surface insolation temperatures near to what they are today, and a new wave of hypervolatile ice sublimation as direct insolation became the dominant steady-state surface heat source.

This is where the curves in Figure 2 apply. Using the same Q_{gas} curves and the insolation energy balance relation $T_{\text{LTE}} = [(1 - A)/\epsilon]^{1/4} 282/\text{sqrt}(r_h) \text{ K}$ for a non- or slowly sublimating body with average albedo A and emissivity ϵ across the solar spectrum, Lisse+21 showed the different spatial regions of stability for the different expected ices (Table 1). As the temperatures of these bodies are raised, the first species to sublime are the most volatile (i.e., the ones that evaporate at the lowest temperatures), and if present at high

Table 1
Ice Stability vs. Sublimation Regions in the Solar System

Solar System Region	T_{LTE} Range ^a (K)	Crystalline Water Ice	Amorphous Water Ice	Other Refractory Ices (CH ₃ OH, HCN, NH ₃ , H ₂ CO, etc.)	Hypervolatiles (N ₂ , CO, CH ₄ , etc.)
Inner System ($r_h < 2.5$ au)	180–5780	Not stable	Not stable	Not stable	Not stable
Outer Asteroid Belt to Saturn ($2.5 < r_h < 10$ au)	90–180	Stable	Not stable	Not stable	Not stable
Saturn to Uranus ($10 < r_h < 20$ au)	60–90	Stable	Stable	Not stable	Not stable
Uranus through Kuiper Belt ($20 < r_h < 70$ au)	35–60	Stable	Stable	Stable	Not stable
Outer Kuiper Belt, Oort Cloud ($r_h \geq 100$ au)	10–20 ^b	Stable	Stable	Stable	Stable

Notes.

^a For a spherical, isothermal graybody. A large, finite, rotating body with different optical and infrared emissivities will have localized surface regions, like the equator and subsolar (noon) point, that will be warmer than T_{LTE} . In other words, there will be variations, both higher and lower, from a single global average temperature depending on the real, physical, and rotational structure of a body, and the strongly nonlinear behavior of the P_{sat} curves of Figure 2 will push the instability regions outward from the Sun from the simple isothermal graybody case.

^b For the Oort Cloud, the Sun's energy input due to insolation is unimportant compared to the energy input from the local galactic ISM heat bath of 10–20 K. Oort Cloud comets spend >99.9% of their time in the galactic ISM.

4

enough relative abundances will sublimatively cool the nucleus and keep its surface temperatures “pinned” near the temperature at which the ice species flash from solid to vapor (i.e., the near-vertical portions of the Q_{gas} curves shown in Figure 2, where the vapor pressure of a given species increases by 20 orders of magnitude in 10 K).

Given this, and allowing for the slower loss rate indicated by Davidsson+21, Prialnik+21, and Steckloff+21 for sublimation from the deep interior of a realistic Arrokoth-like body with inactive lag deposits overlaying the actively sublimating ices, one sees that the hypervolatile ices are only stable on geological and astronomical Gyr timescales at heliocentric distances of 100 au and beyond, in the outer extremes of the Kuiper Belt and in the Oort Cloud region (Figure 2).²⁸ There is simply no way to insulate these cryogenic species versus loss over 4.56 Gyr, given materials known to humankind for KBOs with dayside/nightside surface temperatures of 60/30 K (Bird et al. 2022) and interior core temperatures on the order of 40 K (Lisse+21; Umrhan et al. 2022).

2.3. Late Oort Cloud Formation Implies a Lack of Bulk Hypervolatile Ices

However, compared to observations this presents a puzzle, given that the only Oort Cloud comets known to emit majority hypervolatiles (but little to no refractory volatiles) are Comet C/2016 R2 (Biver et al. 2018; McKay et al. 2019), and perhaps the new hyperdistant active comets such as C/2017 K2 PANSTARRS (Jewitt et al. 2021; Yang et al. 2021). This handful of comets represents a negligible ($\sim 10^{-3}$) fraction of all the known Oort Cloud comets.

The answer lies in the formation timescale for the Oort Cloud. Unlike the Kuiper Belt, which is at or near to the edge of the original protoplanetary disk (PPD), the Oort Cloud is a later construct, formed of billions of icy planetesimals that failed to aggregate onto and become part of one of the giant planets—but were instead scattered out onto nearly hyperbolic, barely bound, million year orbits (Boe et al. 2019). Originally thought to be created quickly during the 1–10 Myr time of greatest mass growth of the giant planets (Duncan et al. 1987), later work has shown (Stern 2003; Dones et al. 2004, 2015; Brasser 2007) that it is very difficult to launch a small planetesimal onto a Myr long, near-unity eccentricity orbit through a midplane dense with gas and other planetesimals, rather than scattering them off of other bodies nearby in the ecliptic. Most current models (e.g., Brasser & Morbidelli 2013; Garrod 2019; Morbidelli & Nesvorny 2020) favor instead the population of the Oort Cloud to start around the time of the giant planet orbital instability, at hundreds of Myr after the beginning of the solar system, via Neptune’s scattering of planetesimals from the Kuiper Belt into the Cloud. The same dynamical processes also removed upwards of 99% of the mass of the Kuiper Belt through ejection and accretion, and created the “dynamically hot” scattered disk KBOs seen in the modern Kuiper Belt (see Nesvorny 2018).

As mentioned above and shown in Figure 2, any small icy solar system body found in regions from the Kuiper Belt inward, including the giant planet region, will lose, via

isolation heating, its hypervolatile majority ices to vacuum within tens of Myr. Since current models have >99% of icy Oort Cloud objects emplaced after hundreds of Myr’s worth of residence time in the giant planet or Kuiper Belt regions, they will have lost their bulk majority hypervolatiles, so we can expect that the large majority of Oort Cloud objects will lack bulk hypervolatile species like CO, N₂, and CH₄.

2.4. An Illustrative Counterexample? Comet 2016/R2

There could be exceptions to the rule of Oort Cloud hypervolatile-depleted comets. For example, a few (<1%) very extraordinary bodies may have been quickly (in <20 Myr’s time) inserted from the giant planet region. These few bodies, if large ($R_{\text{nuc}} > 5$ km), can then endure thousands of orbits’ worth (i.e., Gyr) of hypervolatile loss upon perihelion passage. (But again, the vast majority, >99% of the icy planetesimals launched into Oort Cloud orbits from the giant planet region, after a ~ 100 Myr delay should contain no icy volatiles, except as minority impurities in refractory ice matrices, reproducing the apparent situation we observe today.)

As suggested in Lisse+21, comet C/2016 R2 may represent just such an important example of an object outgassing as one would expect if it was rich in nearly pure N₂, CO, and CH₄ ice. Such an object would show large amounts of these species in its coma as it moved from the Oort Cloud to inside the Kuiper Belt (<30 au), but would show *no trace* of the most refractory ice species—water—in the coma vapor phase, since the ~ 20 K temperature of the comet’s surface enforced by the hypervolatiles’ latent heat of sublimation means that the vapor pressures of refractory ices, as with the usually dominant water, are negligible—and will remain so until the available hypervolatile solids are exhausted. The lack of water gas production from R2 is very telling—for such an active comet, with $Q_{\text{gas}} \sim Q_{\text{CO}} = 10^{29}$ mol s⁻¹, H₂O is always detected in a comet.²⁹ Adopting the 1.1×10^{28} mol s⁻¹ water upper limit of Biver et al. (2018), and using the observed Q_{CO} production rate of $\sim 1.1 \times 10^{29}$ mol s⁻¹ and the $Q_{\text{N}_2}/Q_{\text{CO}}$ ratio of $\sim 8\%$, we see that $Q_{\text{CO}}/Q_{\text{H}_2\text{O}} > 10$. This $Q_{\text{CO}}/Q_{\text{H}_2\text{O}}$ value is at least 5 times higher than in any other comet observed inside the water ice line at ~ 2.5 au, including disrupted/fragmented/hypervolatile comets exposing their core regions (Section 2.1). Similarly, $Q_{\text{N}_2}/Q_{\text{H}_2\text{O}} > 0.8$ is at least 16 times higher than in other comets, making the simple “comet with strange compositional abundance argument” suggested by Biver et al. (2018) hard to accept for this object. Instead, the observed $Q_{\text{N}_2}/Q_{\text{CO}}$ ratio, indicative of the relative coma abundance of N₂ versus CO, is close to the solar N:C atomic abundance ratio (Anders &

²⁸ This simple long-term thermal analytical line of reasoning is valid because other processes, like the transient heating introduced via galactic cosmic rays, nearby passage of O/B stars, explosion of nearby supernovae, and perihelia passages (Stern 2003), are strictly “surface processes” that only affect the top few meters of an object (Lisse+21).

²⁹ Note that a 10^{29} molecules s⁻¹ level of hypervolatile outgassing is reasonable, and can be supported by a 15 km radius object that is losing molar ($\sim 10^{15}$ molecules cm⁻²) amounts of ice surface every second: $(2\pi R_{\text{nuc}}^2) * (2 \times 10^{15} \text{ cm}^{-2} \text{ s}^{-1}) \sim 3 \times 10^{28}$ molecule s⁻¹. From Lisse+21, the evaporation of 1 mole of CO or N₂ ice requires ~ 7.3 kJ of heat; thus, the amount of hypervolatile cooling from the emission rate of 10^{29} molecules s⁻¹ = 1.6×10^9 moles s⁻¹ is $\sim 1.4 \times 10^9$ J s⁻¹, the same order of magnitude, $(1-0.9) * \pi R_{\text{nuc}}^2 * (0.1 \text{ W cm}^{-2} * (1.0 \text{ au}/2.6 \text{ au})^2) = 1 \times 10^{10}$ W, as the insolation heating that the Sun is delivering to R2’s nucleus (with assumed albedo = 0.90) at 2.6 au. So the observed mass loss rate of R2 being attributed to hypervolatile sublimation makes rough sense if R2 is feverishly sublimating from its entire sunlit surface during the small portion of each 20,000 yr long orbital cycle where it is intensely heated. For a 15 km radius object of $\sim 0.5 \text{ g cm}^{-3}$, with $\sim 7 \times 10^{15}$ kg total mass and current orbital loss rate of $\sim 3 \times 10^7$ s [1 yr] * (28 amu for CO/N₂ * 1.67×10^{-27} kg amu⁻¹) * 1×10^{29} molecule s⁻¹ $\sim 1 \times 10^{11}$ kg should be able to endure $\sim 7 \times 10^4$ more of these kinds of passages before dissipating, comprising another or $\sim 2 \times 10^4$ yr passage⁻¹ * 7×10^4 passages = 1.4 Gyr.

Grevesse 1989; Lodders 2003; Asplund et al. 2005) as one would expect for a mix of PPD ices of true solar abundance.

2.5. A Possible Additional Small Population of Large-KBO Derived Comets

Another class of hypervolatile-rich Oort Cloud insertion models, due mainly to Desch & Jackson (2021), suggests that free-flying hypervolatile-rich fragments of dwarf planet surfaces (such as Pluto’s) can be created via energetic impacts during the 2:1 Jupiter:Saturn resonance epoch, and then scattered into the Oort Cloud along with multitudes of “normal” KBOs. Again the hypervolatile-rich surface fragments will be a very small minority compared to the bulk hypervolatile stripped implanted KBOs ($\sim 0.1\%$), and the ratio $N_{\text{Oort hypervolatile rich}}/N_{\text{Oort normal comet}}$ for this process would be determined by the efficiency of carving out kilometer-sized chunks of differentiated dwarf planet surface and ejecting them into the Kuiper Belt. This ratio could thus be very different than that determined by the low efficiency of dynamically scattering very young (< 20 Myr) planetesimals by the giant planets through the busy, well-populated disk of the very young solar system.

3. Conclusions and Observational Tests

The prediction that Oort Cloud comets should be depleted in majority species hypervolatiles has some important implications for the study of the Oort Cloud. Many of these are directly testable, and include the following:

- The prediction that hypervolatile-rich comets are rare, and thus that abundant hypervolatiles will not be a general characteristic of all comets, despite the current high levels of interest expressed over the phenomenon of ultradistant active comets like C/2017K2 (Jewitt et al. 2017; Hui et al. 2018).
- If the hypervolatile-rich objects came from the lucky few primitive planetesimals scattered by the giant planets, then they must have been emplaced within ~ 20 Myr (Davidsson+21, Prialnik+21, Steckloff+21), and thus represent the first objects in the Oort Cloud, and can potentially provide a direct measurement of CO/N₂/CH₄ ratios in the protoplanetary disk.
- Obtaining good, unbiased statistics on the frequency of hypervolatile-rich Oort Cloud comets (i.e., from $N_{\text{Oort, hypervolatile rich}}/N_{\text{Oort, normal comet}}$) can provide important constraints on models of early (< 20 Myr) versus later (0.05–2.0 Gyr) emplacement of objects into the Oort Cloud from the giant planet region of the solar system.
- If instead, following Desch & Jackson (2021), the hypervolatile-rich Oort Cloud comets are sourced from differentiated KBO surfaces, then they could be roughly coeval with the rest of the Oort Cloud and their frequency $N_{\text{Oort, hypervolatile rich}}/N_{\text{Oort, normal comet}}$ will reflect the proportions of Kuiper Belt dwarf planet surfaces in the era of giant planet instability containing hypervolatile-rich phases, convolved with the efficiency of launching these phases into the Oort Cloud.
- The presented arguments also provide an alternate explanation for the high observed CO levels in interstellar object 2I/Borisov other than the one presented in Bodewits et al. (2020)—i.e., that rather than coming from a hypervolatile CO-rich system versus ours, 2I could

instead simply have been launched early (within the first 20 Myr or so) of its natal system’s history, or is representative of the natal system’s dwarf planet surfaces.

The authors would like to thank NASA for financial support of the New Horizons project that funded this study via funding from contracts NASW-02008 and NAS5- 97271/TaskOrder30, and the entire New Horizons mission team for making the success of the flyby and its groundbreaking data return possible. The authors are also indebted to an anonymous graduate student who attended the “UCLA Planet Lunch Seminar” on 2021 May 7 for the inspiration to write this material up into an article.

ORCID iDs

C. M. Lisse  <https://orcid.org/0000-0002-9548-1526>
 G. R. Gladstone  <https://orcid.org/0000-0003-0060-072X>
 L. A. Young  <https://orcid.org/0000-0002-7547-3967>
 D. P. Cruikshank  <https://orcid.org/0000-0002-0541-5569>
 S. A. Sandford  <https://orcid.org/0000-0002-6034-9816>
 B. Schmitt  <https://orcid.org/0000-0002-1230-6627>
 S. A. Stern  <https://orcid.org/0000-0001-5018-7537>
 H. A. Weaver  <https://orcid.org/0000-0003-0951-7762>
 O. Umurhan  <https://orcid.org/0000-0001-5372-4254>
 Y. J. Pendleton  <https://orcid.org/0000-0001-8102-2903>
 J. T. Keane  <https://orcid.org/0000-0002-4803-5793>
 J. M. Parker  <https://orcid.org/0000-0002-3672-0603>
 R. P. Binzel  <https://orcid.org/0000-0002-9995-7341>
 A. M. Earle  <https://orcid.org/0000-0002-2780-7037>
 M. Horanyi  <https://orcid.org/0000-0002-5920-9226>
 M. El-Maarry  <https://orcid.org/0000-0002-8262-0320>
 A. F. Cheng  <https://orcid.org/0000-0001-5375-4250>
 J. M. Moore  <https://orcid.org/0000-0001-5815-0536>
 W. B. McKinnon  <https://orcid.org/0000-0002-4131-6568>
 W. M. Grundy  <https://orcid.org/0000-0002-8296-6540>
 J. J. Kavelaars  <https://orcid.org/0000-0001-7032-5255>
 I. R. Linscott  <https://orcid.org/0000-0002-4832-4456>
 W. Lyra  <https://orcid.org/0000-0002-3768-7542>
 B. L. Lewis  <https://orcid.org/0000-0002-8984-4319>
 D. T. Britt  <https://orcid.org/0000-0003-1377-813X>
 J. R. Spencer  <https://orcid.org/0000-0003-4452-8109>
 C. B. Olkin  <https://orcid.org/0000-0002-5846-716X>
 R. L. McNutt  <https://orcid.org/0000-0002-4722-9166>
 H. A. Elliott  <https://orcid.org/0000-0003-2297-3922>
 N. Dello-Russo  <https://orcid.org/0000-0002-8379-7304>
 J. K. Steckloff  <https://orcid.org/0000-0002-1717-2226>
 M. Neveu  <https://orcid.org/0000-0002-6220-2869>
 O. Mousis  <https://orcid.org/0000-0001-5323-6453>

References

- A’Hearn, M. F., Belton, M. J. S., Delamere, W. A., et al. 2011, *Sci*, **332**, 1396
 A’Hearn, M. F., Feaga, L. M., Keller, H. U., et al. 2012, *ApJ*, **758**, 29
 Anders, E., & Grevesse, N. 1989, *GeCoA*, **53**, 197
 Asplund, M., Grevesse, N., & Sauval, A. J. 2005, in ASP Conf. Ser. 336, Cosmic Abundances as Records of Stellar Evolution and Nucleosynthesis, ed. F. N. Bash & T. G. Barnes (San Francisco, CA: ASP), 25
 Barucci, M. A., Alvarez-Candal, A., Merlin, F., et al. 2011, *Icar*, **214**, 297
 Barucci, M. A., Brown, M. E., Emery, J. P., & Merlin, F. 2008, in The Solar System Beyond Neptune, ed. M. A. Barucci et al. (Tucson, AZ: Univ. Arizona Press), 143
 Bird, M. K., Linscott, I. R., Tyler, G. L., et al. 2022, *PSJ*, **3**, 109
 Biver, N., Bockelee-Morvan, D., Paubert, G., et al. 2018, *A&A*, **619**, A127
 Bockelee-Morvan, D., & Biver, N. 2016, in IAU Proc. 29A, Astronomy in Focus (Cambridge: Cambridge Univ. Press), 321

- Bockelée-Morvan, D., Crovisier, J., Mumma, M. J., & Weaver, H. A. 2004, in *Comets II*, ed. M. C. Festou, H. U. Keller, & H. A. Weaver (Tucson, AZ: Univ. Arizona Press), 391
- Bodewits, D., Noonan, J. W., Feldman, P. D., et al. 2020, *NatAs*, 4, 867
- Boe, B., Jedicke, R., Meech, K. J., et al. 2019, *Icar*, 333, 252
- Brasser, R., Duncan, M. J., & Levison, H. F. 2007, *Icar*, 191, 413
- Brasser, R., & Morbidelli, A. 2013, *Icar*, 225, 40
- Brown, Michael E. 2012, *AREPS*, 40, 467
- Choukroun, M., Altwegg, K., Kührt, E., et al. 2020, *SSRv*, 216, 44
- Cruikshank, D. P., Roush, T. L., Bartholomew, M. J., et al. 1998, *Icar*, 135, 389
- Davidsson, B. J. R. 2021, *MNRAS*, 505, 5654
- Dello Russo, N., Vervack, R. J., Jr., Weaver, H. A., et al. 2007, *Natur*, 448, 172
- Dello Russo, N., Vervack, R. J., Jr., Weaver, H. A., et al. 2008, *ApJ*, 680, 793
- Desch, S. J., & Jackson, A. P. 2021, *JGRE*, 126, e06807
- DiSanti, M. A., Bonev, B. P., Dello-Russo, N., et al. 2017, *AJ*, 154, 246
- Dones, L., Brasser, R., Kaib, N., & Rickman, H. 2015, *SSRv*, 197, 191
- Dones, L., Weissman, P. R., Levison, H. F., & Duncan, M. J. 2004, in *Comets II*, ed. M. C. Festou, H. U. Keller, & H. A. Weaver (Tucson, AZ: Univ. Arizona Press), 153
- Duncan, M., Quinn, T., & Tremaine, S. 1987, *AJ*, 94, 1330
- Ehrenfreund, P., d'Hendecourt, L., Charnley, S., & Ruitkamp, R. 2001, *JGR*, 106, 33291
- Ercolano, B., & Pascucci, I. 2017, *RSOS*, 4, 170114
- Fornasier, S., Feller, C., Hasselmann, P. H., et al. 2019, *A&A*, 630, A13
- Fornasier, S., Hasselmann, P. H., Barruci, M. A., et al. 2015, *A&A*, 583, A30
- Garrod, R. T. 2019, *ApJ*, 884, 69
- Gladstone, G. R., Lisse, C. M., Young, L. A., et al. 2022, *PSJ*, 3, 111
- Grundy, W., Bird, M. K., Britt, D. T., et al. 2020, *Sci*, 367, aay3705
- Hui, M.-T., Jewitt, D. C., & Clark, D. L. 2018, *AJ*, 155, 25
- Iro, N., Gautier, D., Hersant, F., Bockelée-Morvan, D., & Lunine, J. I. 2003, *Icar*, 161, 511
- Ishii, H. A., Bradley, J. P., Bechtel, H. A., et al. 2018, *PNAS*, 115, 6608
- Jewitt, D. C. 2009, *AJ*, 137, 4296
- Jewitt, D. C., Hui, M.-T., Mutchler, M., et al. 2017, *ApJL*, 847, L19
- Jewitt, D. C., Kim, Y., Mutchler, M., et al. 2021, *AJ*, 161, 188
- Kral, Q., Pringle, J. E., Guilbert-Lepoutre, A., et al. 2021, *A&A*, 653, L11
- Li, J., Jewitt, D., Mutchler, M., Agarwal, J., & Weaver, H. 2020, *AJ*, 159, 209
- Lisse, C. M. 2002, *EM&P*, 90, 497
- Lisse, C. M., Sitko, M. L., Marengo, M., et al. 2017, *AJ*, 154, 182
- Lisse, C. M., Young, L. A., Cruikshank, D. P., et al. 2021, *Icar*, 356, 114072
- Lodders, K. 2003, *ApJ*, 591, 1220
- McKay, A. J., DiSanti, M. A., Kelley, M. S. P., et al. 2019, *AJ*, 158, 128
- Meech, K. J., Pittichová, J., Bar-Nun, A., et al. 2009, *Icar*, 201, 719
- Morbidelli, A., & Nesvorný, D. 2020, in *The Trans-Neptunian Solar System*, ed. D. Prialnik, M. A. Barucci, & L. A. Young (Amsterdam: Elsevier), 25
- Mumma, M. J., & Charnley, S. 2011, *ARA&A*, 49, 471
- Nesvorný, D. 2018, *ARA&A*, 56, 137
- Prialnik, D. 2021, *BAAS*, 53, 2021n7i307p10
- Prialnik, D., Bar-Nun, A., & Podolak, M. 1987, *ApJ*, 319, 993
- Prialnik, Dina, & Bar-Nun, Akiva 1990, *ApJ*, 355, 281
- Prialnik, D., & Bar-Nun, A. 1992, *A&A*, 258, L9
- Quirico, E., Moroz, L.V., Beck, P., et al. 2015, *EPSC*, EPSC2015-621
- Quirico, E., Moroz, L.V., Schmitt, B., et al. 2016, *Icar*, 272, 32
- Schaller, E. L., & Brown, M. E. 2007, *ApJ*, 659, L61
- Steckloff, J. K., Graves, K., Hirabayashi, M., Melosh, H. J., & Richardson, J. E. 2016, *Icar*, 272, 60
- Steckloff, J. K., Johnson, B. C., & Bowling, T. 2015, *Icar*, 258, 430
- Steckloff, J. K., Lisse, C. M., Safrit, T. K., et al. 2021, *Icar*, 356, 113998
- Steckloff, J. K., & Samarasingha, N. H. 2018, *Icar*, 312, 172
- Stern, S. A. 2003, *Natur*, 424, 639
- Stern, S. A., Weaver, H. A., Spencer, J. R., et al. 2019, *Sci*, 364, 9771
- Sunshine, J. M., A'Hearn, M. F., Groussin, O., et al. 2006, *Sci*, 311, 1453
- Umruhan, O., Grundy, W., Bird, M., et al. 2022, *PSJ*, 3, 110
- Williams, J. P., & Cieza, L. A. 2011, *ARA&A*, 49, 67
- Yang, B., Jewitt, D. C., Zhao, Y., et al. 2021, *ApJL*, 914, L17
- Young, L. A., Braga-Ribas, F., & Johnson, R. E. 2020, in *The Trans-Neptunian Solar System*, ed. D. Prialnik, M. A. Barucci, & L. Young (Amsterdam: Elsevier), 127
- Zahnle, K. J., & Catling, D. C. 2017, *ApJ*, 843, 122
- Zhukovska, S., Henning, T., & Dobbs, C. 2018, *ApJ*, 857, 2